Supplementary material for

The 8.2 ka event in Northern Spain: timing, structure and climatic impact from a multi-proxy speleothem record

Hege Kilhavn[1,2], Isabelle Couchoud[1,2], Russell N. Drysdale[2], Carlos Rossi[3], John Hellstrom[2], Fabien Arnaud[1], Henri Wong[4]

[1]EDYTEM, Université Savoie Mont Blanc, 73376 Le Bourget du Lac, France
[2]School of Geography, Earth and Atmospheric Sciences, The University of Melbourne, 3010 Victoria, Australia
[3]Dept. Petrología y Geoquímica, Facultad de Ciencias Geológicas, Universidad Complutense, 28040 Madrid, Spain
[4]Australian Nuclear Science and Technology Organisation, Lucas Heights, NSW 2234, Australia

Correspondence to: Hege Kilhavn (hege.kilhavn@univ-smb.fr)

Content of supplementary material

Table S1. Uranium-series analyses from stalagmite SIR-14. Activity ratios were determined following the procedure of Hellstrom (2003). The ages (ka BP) is corrected for initial ^{230}Th using equation 1 of Hellstrom (2006), the decay constants of Cheng et al. (2013) and an initial activity ratio of ^{230}Th/^{232}Th of 2.7 ± 0.9 using the stratigraphic constraint method of Hellstrom (2006). All uncertainties are 2σ. Sample SIR-14-D-145* (red font), have been discarded as an outlier.

Sample ID	Depth from top (mm)	Mass (g)	^{238}U (ng g^{-1})	^{230}Th/^{238}U activity ratio	^{234}U/^{238}U activity ratio	^{232}Th/^{238}U activity ratio	^{230}Th/^{232}Th activity ratio	Age ka (uncorrected)	^{230}Th/^{232}Th initial activity ratio	Age ka BP (1950) (corrected)	^{234}U/^{238}U initial activity ratio (corrected)
SIR-14-1	6.5 ± 2.0	0.02	300	0.0873 ± 0.0012	1.3493 ± 0.0048	0.003585 ± 0.000090	24.3	7.274 ± 0.107	2.7 ± 0.9	6.426 ± 0.281	1.3557 ± 0.0048
SIR-14-19-29	28.5 ± 2.0	0.05	285	0.0813 ± 0.0008	1.3680 ± 0.0028	0.000149 ± 0.000003	545.1	6.654 ± 0.070	2.7 ± 0.9	6.563 ± 0.069	1.3749 ± 0.0028
SIR-14-19-50	49.5 ± 2.0	0.05	283	0.0831 ± 0.0007	1.3769 ± 0.0027	0.000111 ± 0.000002	751.5	6.754 ± 0.060	2.7 ± 0.9	6.677 ± 0.060	1.3841 ± 0.0027
SIR-14-19-73	71.5 ± 2.0	0.05	192	0.0889 ± 0.0010	1.3579 ± 0.0029	0.000134 ± 0.000003	665.5	7.351 ± 0.083	2.7 ± 0.9	7.264 ± 0.087	1.3653 ± 0.0029
SIR-14-2	72.5 ± 2.0	0.02	164	0.1012 ± 0.0019	1.3449 ± 0.0045	0.004243 ± 0.000108	23.8	8.503 ± 0.168	2.7 ± 0.9	7.507 ± 0.353	1.3524 ± 0.0046
SIR-14-19-87	84.5 ± 2.0	0.05	215	0.0960 ± 0.0009	1.3548 ± 0.0029	0.000113 ± 0.000002	850.2	8.019 ± 0.083	2.7 ± 0.9	7.896 ± 0.081	1.3629 ± 0.0030
SIR-14-19-96	93.5 ± 2.0	0.05	272	0.0970 ± 0.0008	1.3564 ± 0.0027	0.000025 ± 0.000001	3838.3	8.044 ± 0.073	2.7 ± 0.9	7.991 ± 0.070	1.3646 ± 0.0027
SIR-14-19-105	102.5 ± 2.0	0.05	295	0.0982 ± 0.0008	1.3599 ± 0.0027	0.000085 ± 0.000002	1160.5	8.147 ± 0.074	2.7 ± 0.9	8.060 ± 0.071	1.3683 ± 0.0028
SIR-14-19-131	127.5 ± 2.0	0.05	326	0.0991 ± 0.0008	1.3559 ± 0.0027	0.000385 ± 0.000008	257.3	8.224 ± 0.070	2.7 ± 0.9	8.098 ± 0.076	1.3642 ± 0.0027
SIR-14-D-138	133.5 ± 4.0	0.04	299	0.0999 ± 0.0007	1.3519 ± 0.0028	0.000193 ± 0.000004	519.6	8.345 ± 0.063	2.7 ± 0.9	8.232 ± 0.065	1.3602 ± 0.0029
SIR14-D-145*	138.5 ± 2.0	0.05	265	0.1022 ± 0.0013	1.3501 ± 0.0029	0.000040 ± 0.000001	2529.9	8.556 ± 0.115	2.7 ± 0.9	8.477 ± 0.115	1.3587 ± 0.0029
SIR-14-D-153	146.5 ± 4.0	0.06	289	0.1000 ± 0.0006	1.3465 ± 0.0031	0.000118 ± 0.000002	850.3	8.389 ± 0.056	2.7 ± 0.9	8.292 ± 0.056	1.3547 ± 0.0032
SIR-14-D-165	158.5 ± 4.0	0.05	319	0.1023 ± 0.0007	1.3558 ± 0.0026	0.000134 ± 0.000003	765.1	8.527 ± 0.063	2.7 ± 0.9	8.428 ± 0.064	1.3644 ± 0.0026
SIR-14-19-176	169.5 ± 2.0	0.05	306	0.1037 ± 0.0009	1.3638 ± 0.0028	0.000085 ± 0.000002	1212.7	8.645 ± 0.079	2.7 ± 0.9	8.508 ± 0.079	1.3727 ± 0.0029
SIR14-D-211	203.5 ± 2.0	0.05	292	0.1075 ± 0.0013	1.3545 ± 0.0028	0.000040 ± 0.000001	2661.1	8.989 ± 0.113	2.7 ± 0.9	8.906 ± 0.114	1.3636 ± 0.0028
SIR-14-19-252	244.5 ± 2.0	0.05	348	0.1106 ± 0.0009	1.3676 ± 0.0027	0.000044 ± 0.000001	2521.2	9.181 ± 0.075	2.7 ± 0.9	9.085 ± 0.080	1.3772 ± 0.0028
SIR14-D-256	248.5 ± 2.0	0.05	174	0.1128 ± 0.0016	1.3498 ± 0.0033	0.000144 ± 0.000003	785.1	9.482 ± 0.146	2.7 ± 0.9	9.381 ± 0.143	1.3593 ± 0.0034
SIR-14-3	254.5 ± 2.0	0.02	220	0.1201 ± 0.0015	1.3520 ± 0.0048	0.001897 ± 0.000058	63.3	10.105 ± 0.137	2.7 ± 0.9	9.628 ± 0.195	1.3618 ± 0.0049
SIR-14-19-279	270.5 ± 2.0	0.04	362	0.1194 ± 0.0009	1.3549 ± 0.0027	0.000067 ± 0.000001	1792	10.024 ± 0.084	2.7 ± 0.9	9.938 ± 0.083	1.3651 ± 0.0027

Sample ID	Depth from top (mm)	Mass (g)	^{238}U (ng g^{-1})	$^{230}Th/^{238}U$ activity ratio	$^{234}U/^{238}U$ activity ratio	$^{232}Th/^{238}U$ activity ratio	$^{230}Th/^{232}Th$ activity ratio	Age ka (uncorrected)	$^{230}Th/^{232}Th$ initial activity ratio	Age ka BP (1950) (corrected)	$^{234}U/^{238}U$ initial activity ratio (corrected)
SIR-14-19-358	350.5 ± 2.0	0.05	393	0.1276 ± 0.0008	1.3536 ± 0.0026	0.000045 ± 0.000001	2810	10.818 ± 0.076	2.7 ± 0.9	10.674 ± 0.074	1.3645 ± 0.0027
SIR-14-4	*412.5 ± 2.0*	*0.02*	*375*	*0.1524 ± 0.0012*	*1.4571 ± 0.0043*	*0.001058 ± 0.000029*	*144.1*	*11.980 ± 0.106*	*2.7 ± 0.9*	*11.701 ± 0.127*	*1.4725 ± 0.0044*

Table S2. The five new uranium-series analyses from stalagmite SIR-1. The new dating samples were measured from stalagmite SIR-1 (Rossi et al., 2018) to improve the chronology in the early Holocene part of this sample. Activity ratios were determined following the procedure of Hellstrom (2003). The ages (ka BP) is corrected for initial ^{230}Th using equation 1 of Hellstrom (2006), the decay constants of Cheng et al. (2013). The initial activity ratio of $^{230}Th/^{232}Th$ was originally set to 1.5 ± 1.5 (Rossi et al., 2018). This was revised by using the stratigraphic constraint method of Hellstrom (2006), which yielded inconclusive results. Stalagmite SIR-14 gave redundant results, and, therefore we applied the same initial $^{230}Th/^{232}Th$ activity ratio to the SIR-1 samples (2.7 ± 0.9). All uncertainties are 2σ. There are several outliers in this stalagmite (red font), most of them are related to uranium loss and open system behaviour, but two of them have high detrital contamination.

| Sample ID	Depth from top (mm)	Mass (g)	^{238}U (ng g^{-1})	$^{230}Th/^{238}U$ activity ratio	$^{234}U/^{238}U$ activity ratio	$^{232}Th/^{238}U$ activity ratio	$^{230}Th/^{232}Th$ activity ratio	Age ka (uncorrected)	$^{230}Th/^{232}Th$ initial activity ratio	Age ka BP (1950) (corrected)	$^{234}U/^{238}U$ initial activity ratio (corrected)
SIR-1-18.45	18.5 ± 2.0	0.04	250	0.1024 ± 0.0016	1.3458 ± 0.0033	0.000292 ± 0.000006	350.4	8.602 ± 0.141	2.7 ± 0.9	8.464 ± 0.142	1.3543 ± 0.0034
SIR-1-36.56	36.6 ± 2.0	0.04	260	0.0995 ± 0.0017	1.3430 ± 0.0034	0.000188 ± 0.000004	528.7	8.368 ± 0.148	2.7 ± 0.9	8.254 ± 0.147	1.3512 ± 0.0035
SIR-1-40.01	40.0 ± 2.0	0.04	273	0.1175 ± 0.0015	1.3451 ± 0.0030	0.000393 ± 0.000008	298.8	9.930 ± 0.134	2.7 ± 0.9	9.775 ± 0.140	1.3548 ± 0.0032
SIR-1-54.80	54.8 ± 2.0	0.04	291	0.1041 ± 0.0014	1.3403 ± 0.0030	0.000210 ± 0.000004	496.3	8.788 ± 0.124	2.7 ± 0.9	8.674 ± 0.123	1.3488 ± 0.0030
SIR-1-72.65	72.7 ± 2.0	0.04	227	0.1063 ± 0.0015	1.3369 ± 0.0031	0.000739 ± 0.000015	143.9	9.004 ± 0.134	2.7 ± 0.9	8.774 ± 0.145	1.3455 ± 0.0032
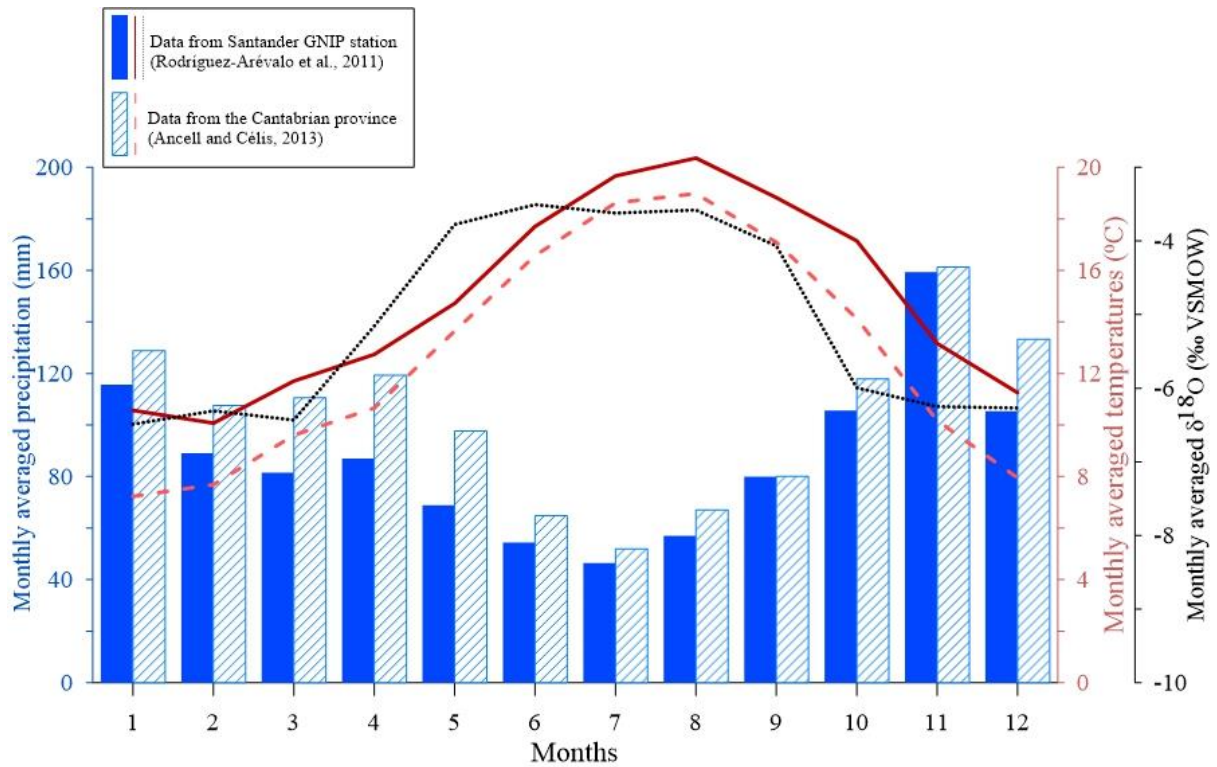
Figure S1. Weather data from the Cantabrian region in Northern Spain. Monthly averaged precipitation and temperature from the nearest GNIP station, Santander (Rodríguez-Arévalo et al., 2011) and averaged precipitation and temperature across the Cantabrian province (Ancell and Célis, 2013). The data from the Santander GNIP station are shown as: monthly averaged precipitation = dark blue columns, monthly averaged temperature = dark red line and monthly averaged $\delta^{18}O$ of precipitation = black, dotted line. The averaged data across the Cantabrian province are shown as: monthly averaged precipitation = light blue slashed columns and monthly averages temperature = red, stapled line. Number of months is referred to as 1 = January, 2 = February, and following.
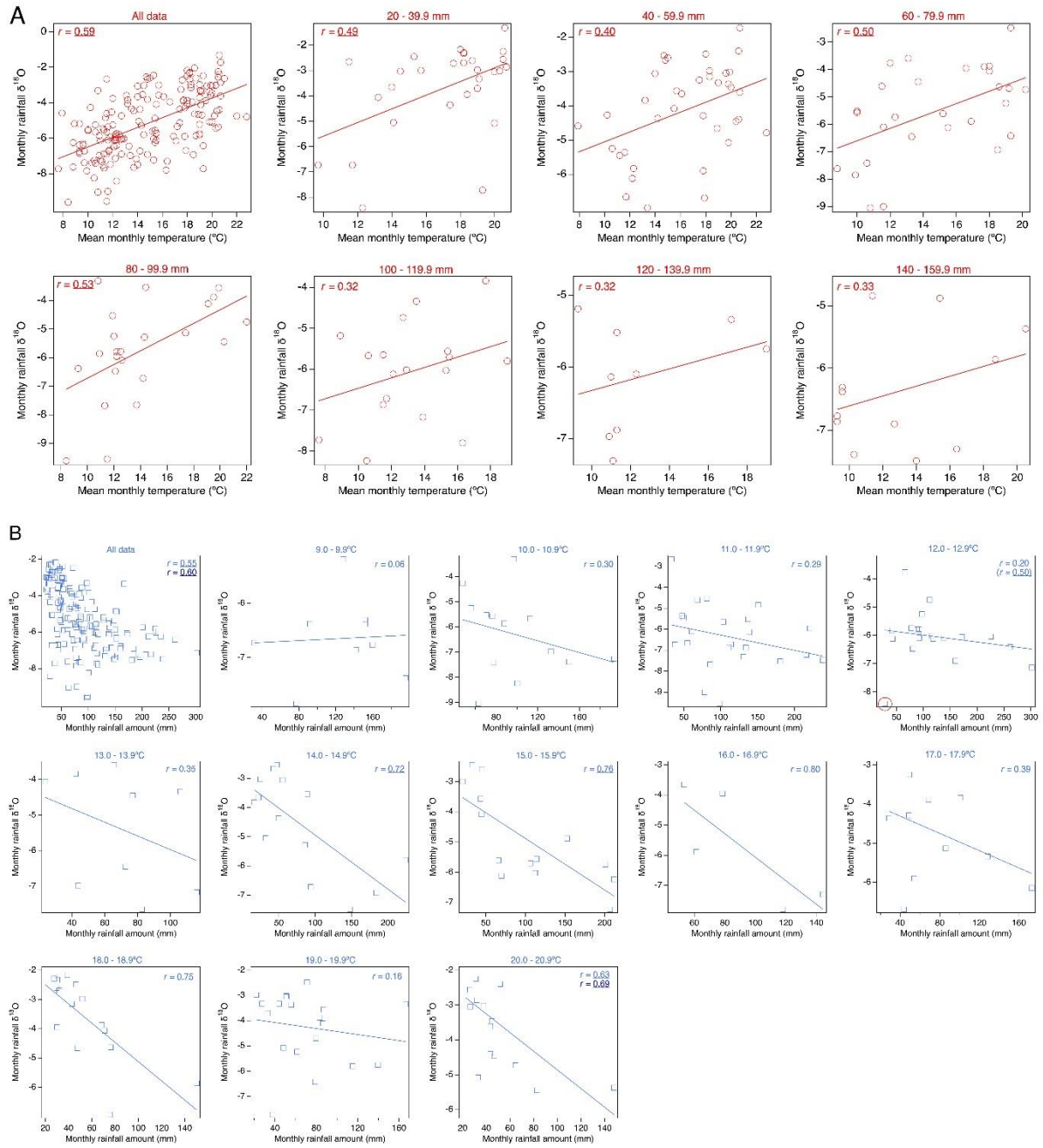
Figure S2. Deconvolution of monthly rainfall $\delta^{18}O$, rainfall amount and mean temperature data from the Santander Global Network of Isotopes in Precipitation (GNIP) collection station for the period 2000-2015 CE. At the aggregate level, rainfall $\delta^{18}O$ shows a statistically significant correlation with both temperature ('All data', upper left panel of A) and rainfall amount ('All data', upper left panel of B). However, due to the predominance of winter precipitation in the region, either or both of the 'temperature effect' and 'rainfall amount effect' may be spurious. Stratifying the data by rainfall amount (remaining panels shown in A) and temperature (remaining panels shown in B) enables one to examine the rainfall $\delta^{18}O$ vs temperature effect and rainfall $\delta^{18}O$ vs rainfall amount effect respectively by keeping the other variable ~constant. In A, the data are stratified into 20 mm rainfall class intervals; in B, the data are stratified into 1ºC temperature classes. Lines of best fit are shown. Statistically significant Pearson r correlation coefficients are underlined. In B, the higher r values shown in dark blue in the first and last panels are based on a log-linear fit ($\log_{10}$ of rainfall), whilst the r value in brackets (0.50) in the last panel of the first row is the correlation coefficient with the circled outlier removed. Based on the data available, the results suggest that neither the rainfall amount effect nor the temperature effect are a persistent influence on

rainfall $\delta^{18}O$ but are rather transient features, highlighting the complexity in interpreting regional rainfall $\delta^{18}O$ values and, consequently, speleothem $\delta^{18}O$ values.

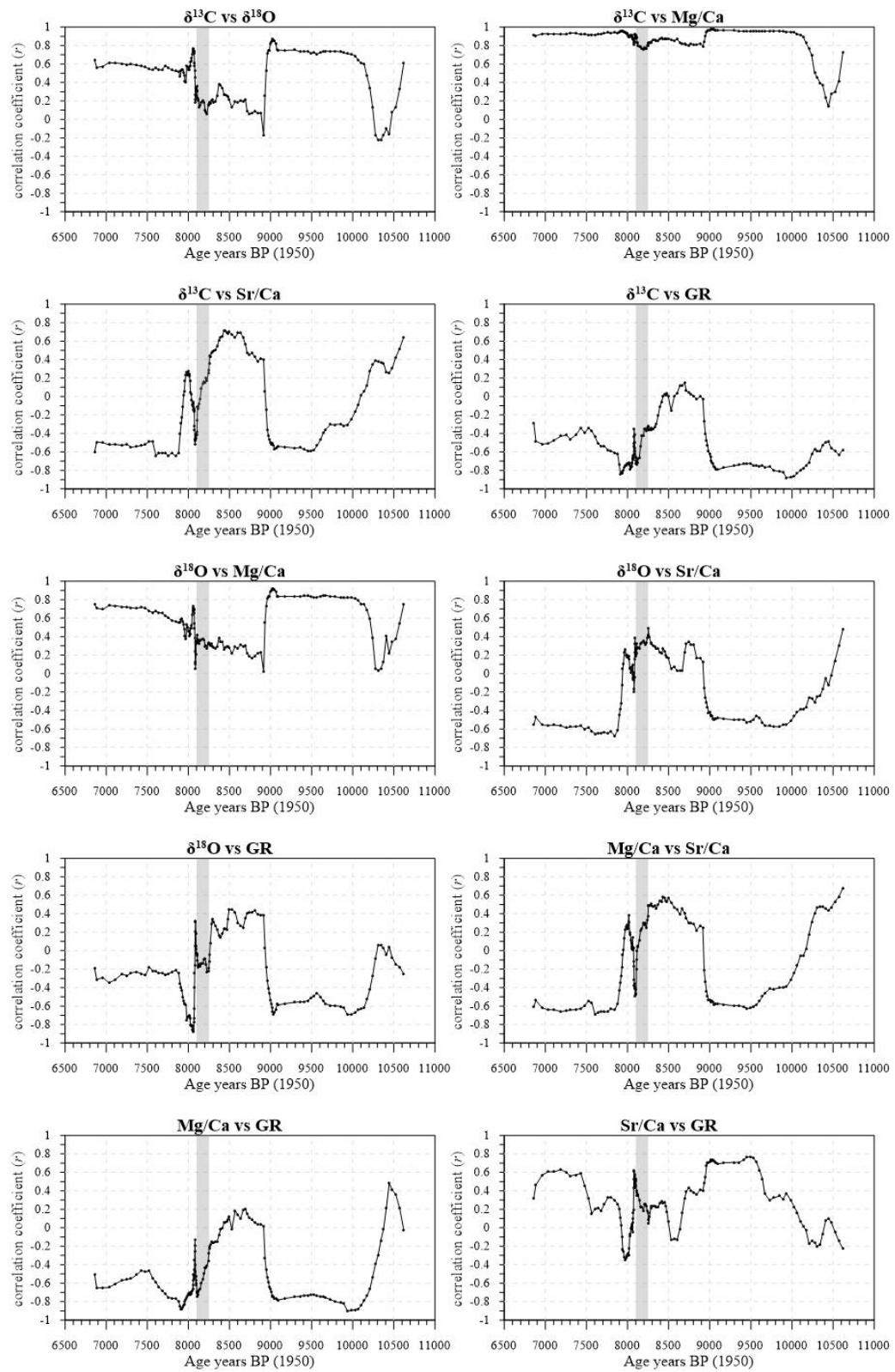**Figure S3**. The 30-point running correlation coefficients for the measured proxies in stalagmite SIR-14 (δ^{13}C, δ^{18}O, Mg/Ca, Sr/Ca and growth rate (GR)). This highlights time intervals of higher positive (and negative) correlation. The grey-shaded area shows the duration of the 8.2 ka event from the NGRIP ice-core record (Thomas et al., 2007).
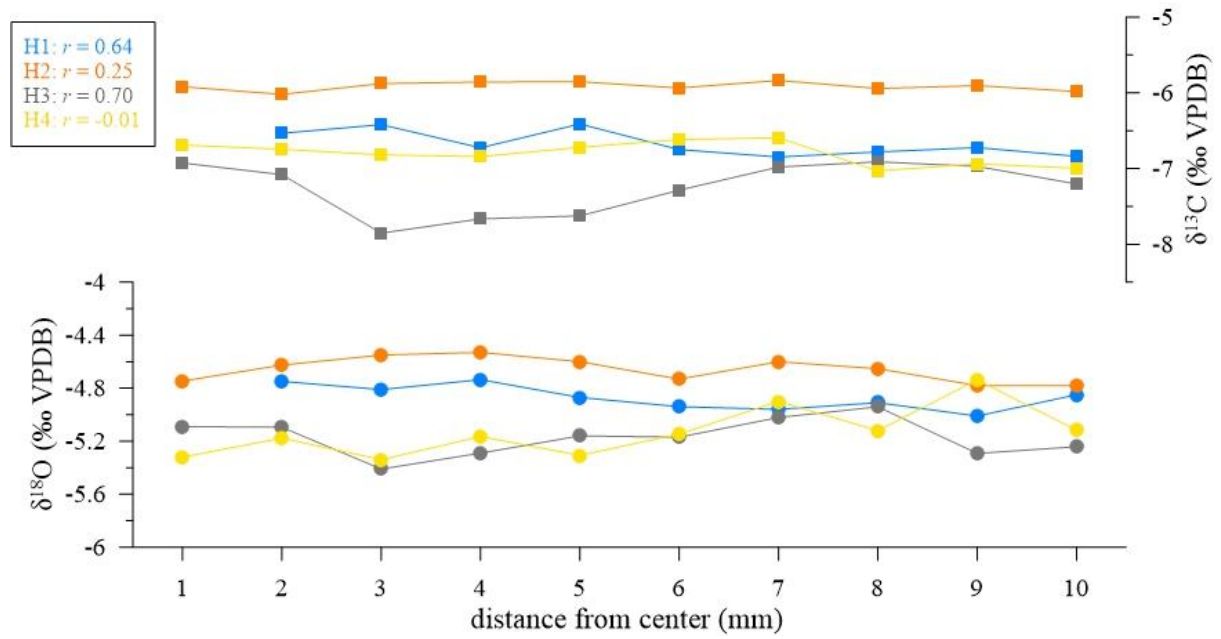
Figure S4. $\delta^{18}O$ (circles) and $\delta^{13}C$ (squares) measurements along single laminae in SIR-14 (Hendy test: Hendy, 1971), each plotted on their respective axes. Each lamina is shown by a unique colour (H1 = blue, H2 = orange, H3 = grey, H4 = yellow), and its location is marked with the same numbers (H1-H4) in fig. 3 (in the manuscript). Lamina H2 and H4 are not correlated; however, lamina H1 and H3 have a moderate correlation. There is a scatter of values in the $\delta^{18}O$ within a single lamina (up to 0.6 ‰), however, there is no clear trend of enrichment from the central axis zone towards the flanks of the stalagmite.
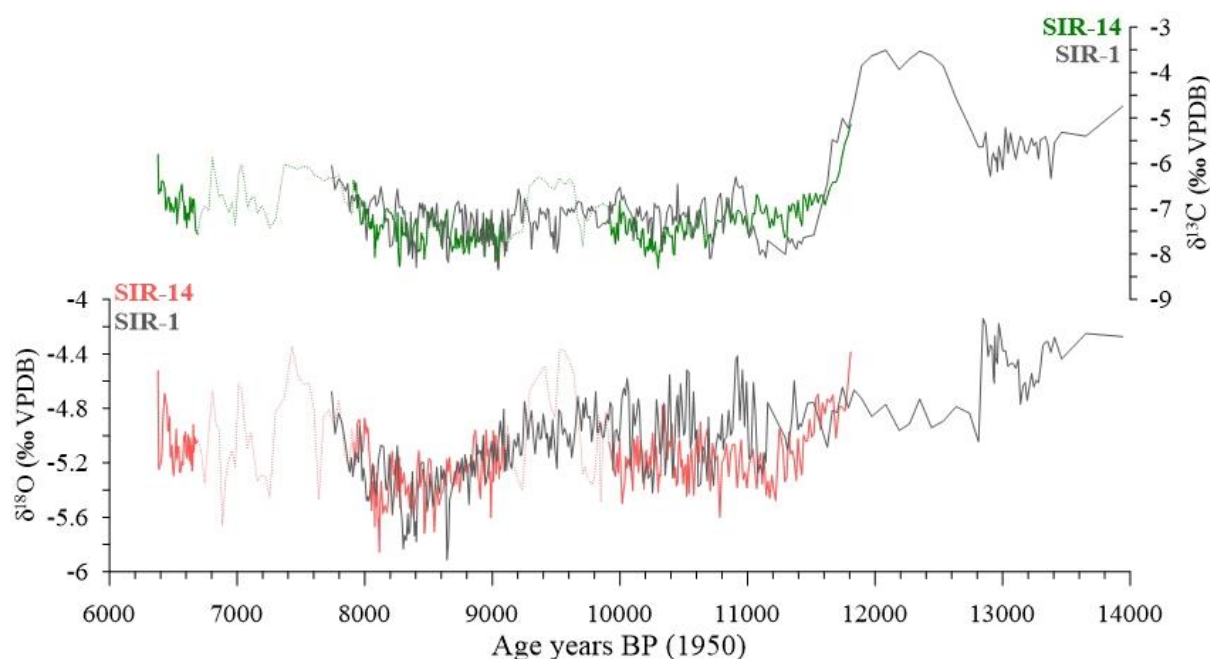
Figure S5. Comparison between stalagmite SIR-14 and SIR-1 isotope records. Overall, the δ¹⁸O and δ¹³C records of SIR-14 replicates well with the SIR-1 isotope records. However, SIR-1 does not replicate the oldest slow-growth interval recorded in SIR-14 (see sect. 5.1.1 in the manuscript). This is explained as a localised perturbation of infiltration at that specific drip site. The 8.2 ka event is also absent in the SIR-1 record. We hypothesize that this could be due to the fact that SIR-1 has several outliers (age-inversions) which potentially could put the record slightly out of phase, with the excursion at ~8.4 ka BP potentially recognised as the 8.2 ka event. However, this remains unknown, and cannot be resolved due to SIR-1's complex U-Th age results and derived age model.
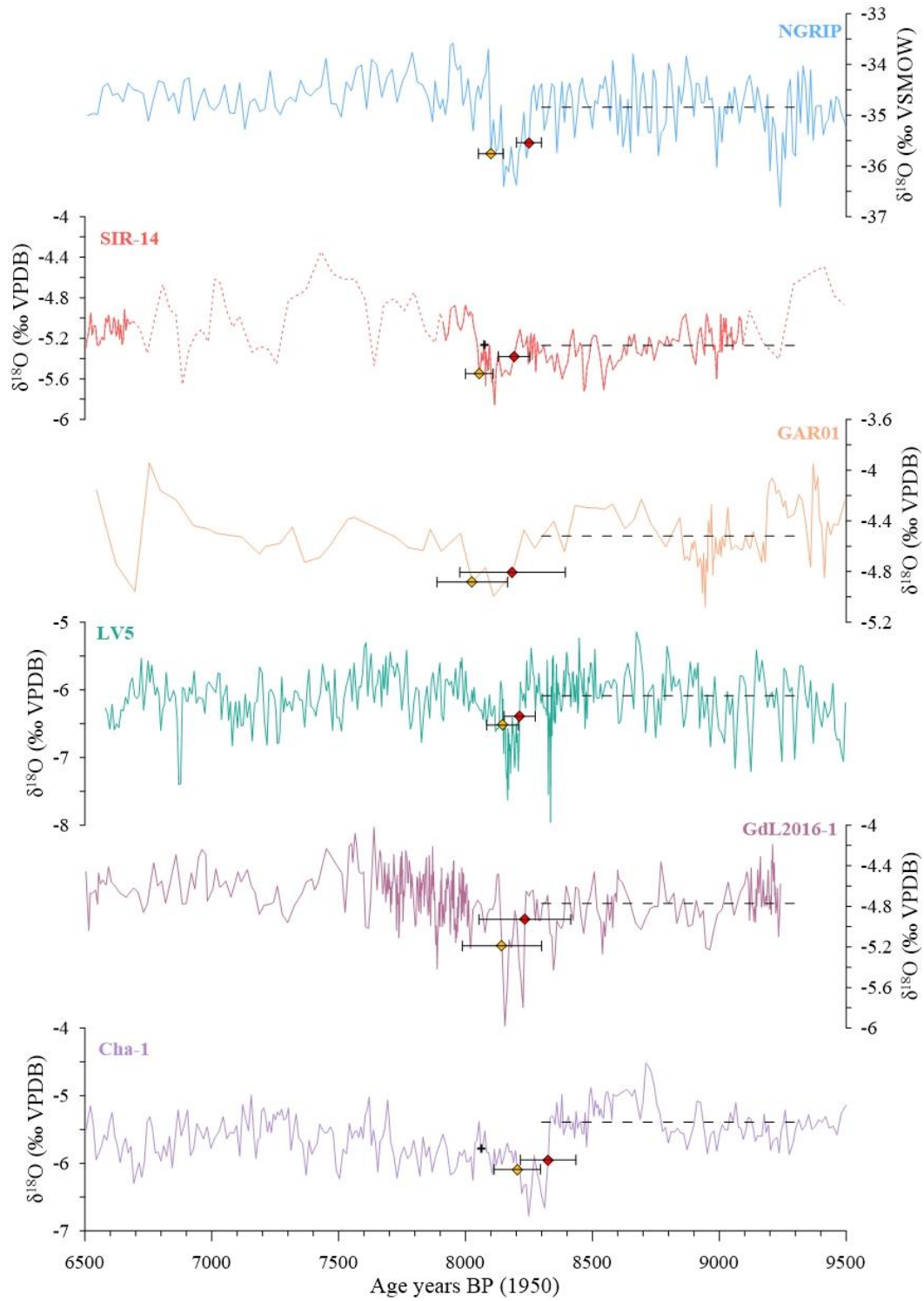
Figure S6. Identification of the 8.2 ka event in various archives. The final defined onset and end of the event is shown by red and yellow markers, respectively. Initially, we used the statistical approach by Thomas et al. (2007) to define the duration of the event, where the onset (end) of the 8.2 ka event is defined as the first (last) isotopic data point below the baseline (stapled black line) that precedes the event (Thomas et al., 2007). In cases where the position of the onset/end did not visually match the structure of the event in the NGRIP ice core, the onset/end isotopic data point was shifted to a structurally similar position. The statistically defined isotopic points for the onset (end) are marked as black circles (black crosses) to show the initial position before moving it to its position based on visual observation.
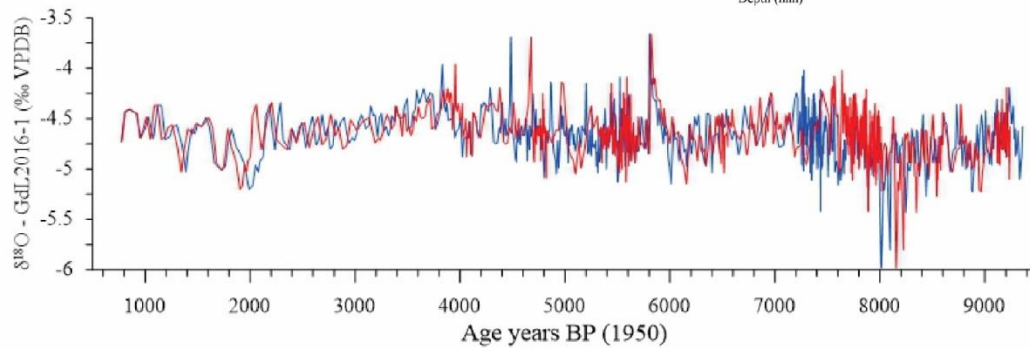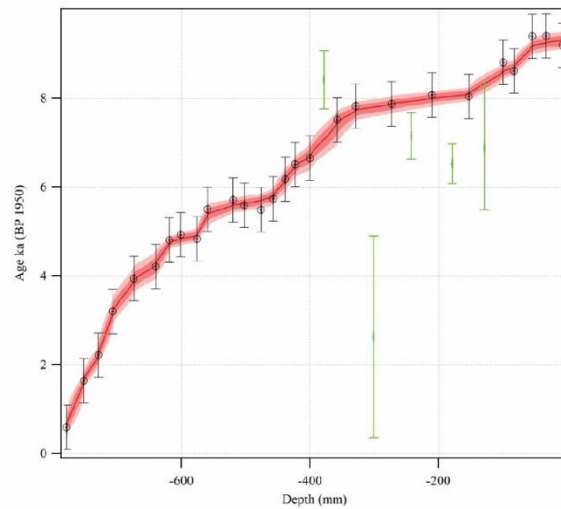
(A)

GAR01

La Garma Cave, Spain
Baldini et al. (2015; 2019)
GR tolerance = 1.0 ± 0.4
$^{230}Th/^{232}Th = 1.2 \pm 1.2$
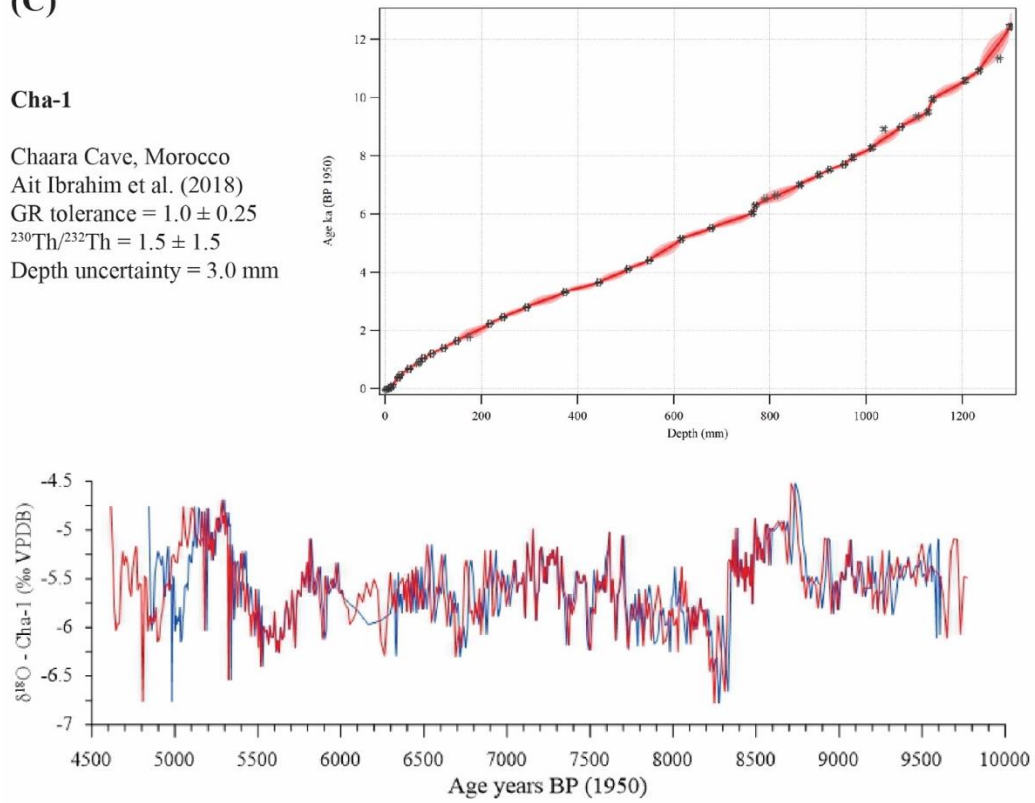Depth uncertainty = 1.0-2.5 mm
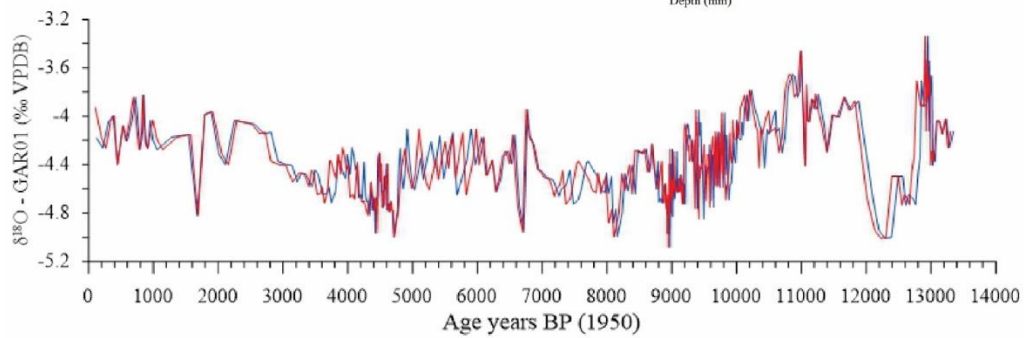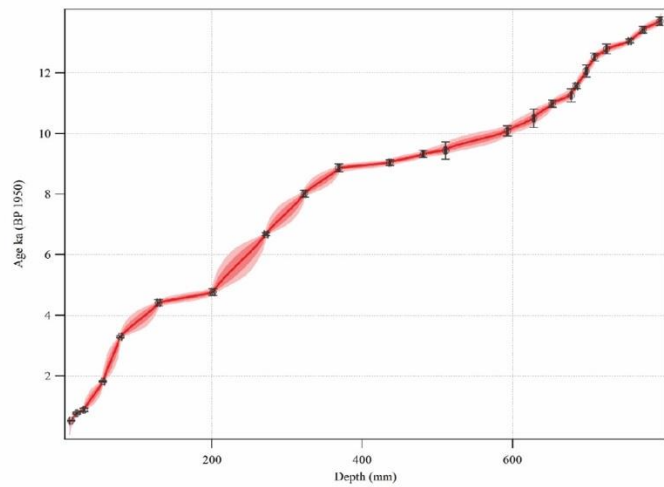
(B)

GdL2016-1

Galeria das Lâminas, Portugal
Benson et al. (2021)
GR tolerance = 1.1 ± 0.3
$^{230}Th/^{232}Th = 0.6 \pm 0.2$
Depth uncertainty = 0.5 mm

(C)

Cha-1

Chaara Cave, Morocco
Ait Ibrahim et al. (2018)
GR tolerance = 1.0 ± 0.25
^{230}Th/^{232}Th = 1.5 ± 1.5
Depth uncertainty = 3.0 mm

(D)

SIR-1

El Soplao Cave, Spain
Rossi et al. (2018)
GR tolerance = 1.2 ± 0.25
^{230}Th/^{232}Th = 2.7 ± 0.9
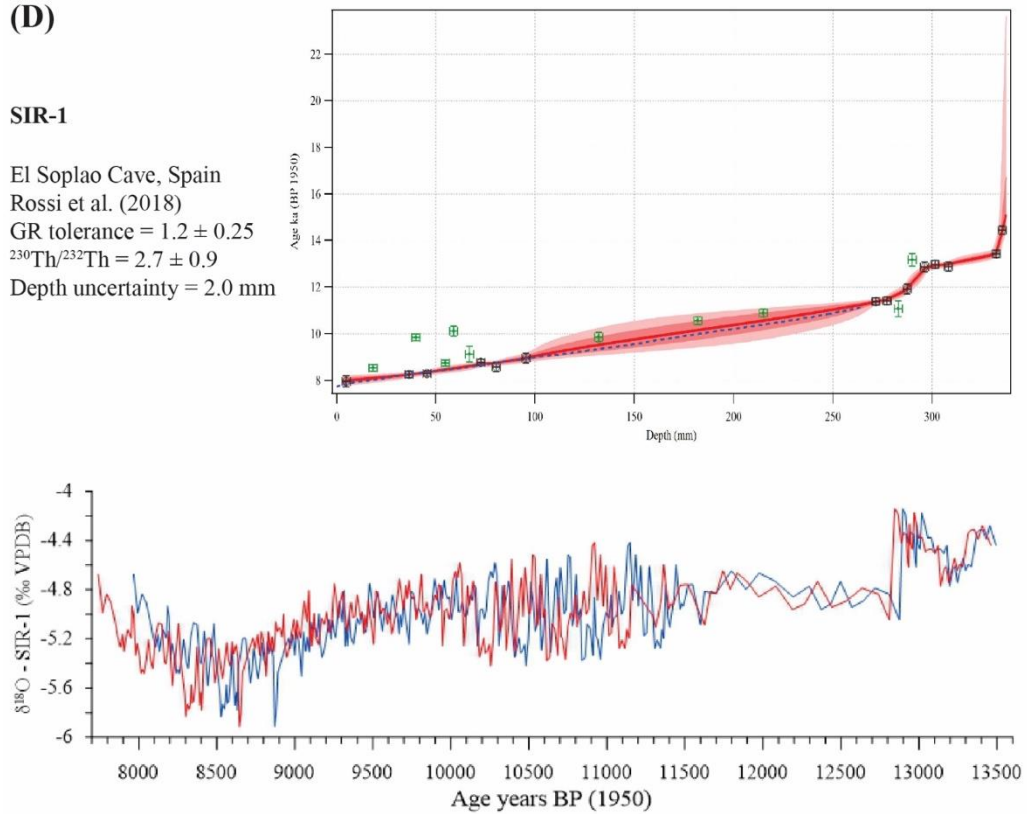Depth uncertainty = 2.0 mm

Figure S7. The chronology of each record was reconstructed using the *Finite-positive-growth-rate model* (Corrick et al., 2020) in order to avoid potential methodological bias in age-depth modelling. The red envelopes represent the 66 % and 95 % confidence intervals, the U-Th dates are marked with black symbols (green symbols for outliers). The standardisation of U-Th ages and age-depth modelling resulted in minor changes in the chronology as shown in the plot of revised time series (red) and original time series (blue). A) stalagmite GAR01 (La Garma Cave: Baldini et al., 2015 ;2019), B) stalagmite GdL-2016-1 (Galeria das Lâminas: Benson et al., 2021), C) stalagmite Cha-1 (Chaara Cave: Ait Ibrahim et al., 2018), D) stalagmite SIR-1 (El Soplao Cave: Rossi et al., 2018). In D) five new dating samples were drilled between 18.45 and 72.65 mm from the top in stalagmite SIR-1 to improve the chronology of the early Holocene part. The originally published estimate of initial $^{230}Th/^{232}Th$ ratio was revised using the stratigraphic constraint method of Hellstrom (2006). This gave inconclusive results, only suggesting that the initial $^{230}Th/^{232}Th$ ratio was less than 4.5. Based on the redundant stratigraphic constraint of stalagmite SIR-14, which is located in the same cave passage (~5 m apart), we assume initial $^{230}Th/^{232}Th$ ratio to be 2.7 ± 0.9 for stalagmite SIR-1, as for SIR-14. There are several potential outliers (green) in this stalagmite, some due to localized open system behaviour (U-leaching) and some due to contamination. The relative position of SIR-1 compared to SIR-14 makes it more exposed to occasional flooding, which could be one explanation for the contamination and age-inversions. After the revision of the age-depth model, the floating lamina chronology (blue dotted line) was anchored to the absolute age that minimises the differences between the lamina chronology and the U-Th dates. The new floating lamina chronology was moved back 226 years compared to the published record (Rossi et al., 2018).

References

Ait Brahim, Y., Wassenburg, J.A., Sha, L., Cruz, F.W., Deininger, M., Sifeddine, A., Bouchaou, L., Spötl, C., Edwards, R.L. & Cheng, H. 2019. North Atlantic Ice-Rafting, Ocean and Atmospheric Circulation During the Holocene: Insights From Western Mediterranean Speleothems. *Geophysical Research Letters,* 46 (13), pp. 7614-7623. https://doi.org/10.1029/2019GL082405.

Ancell, R. & Célis, R. 2013. Termopluviometría de Cantabria durante el periodo 1981-2010. Agencia Estatal de Meteorología (AEMET), nota técnica no. 10. NIPO: 281-12-014-0; 20.

Baldini, L.M., Baldini, J.U.L., McDermott, F., Arias, P., Cueto, M., Fairchild, I.J., Hoffmann, D.L., Mattey, D.P., Müller, W., Nita, D.C., Ontañón, R., Garciá-Moncó, C. & Richards, D.A. 2019. North Iberian temperature and rainfall seasonality over the Younger Dryas and Holocene. *Quaternary Science Reviews,* 226. https://doi.org/10.1016/j.quascirev.2019.105998.

Benson, A., Hoffmann, D.L., Daura, J., Sanz, M., Rodrigues, F., Souto, P. & Zilhão, J. 2021. A speleothem record from Portugal reveals phases of increased winter precipitation in western Iberia during the Holocene. *The Holocene,* 31 (8), pp. 1339-1350. https://doi.org/10.1177/09596836211011666.

Cheng, H., Lawrence Edwards, R., Shen, C.-C., Polyak, V.J., Asmerom, Y., Woodhead, J., Hellstrom, J., Wang, Y., Kong, X., Spötl, C., Wang, X. & Calvin Alexander, E. 2013. Improvements in 230Th dating, 230Th and 234U half-life values, and U–Th isotopic measurements by multi-collector inductively coupled plasma mass spectrometry. *Earth and Planetary Science Letters,* 371-372, pp. 82-91. https://doi.org/10.1016/j.epsl.2013.04.006.

Corrick, E.C., Drysdale, R.N., Hellstrom, J.C., Capron, E., Rasmussen, S.O., Zhang, X., Fleitmann, D., Couchoud, I. & Wolff, E. 2020. Synchronous timing of abrupt climate changes during the last glacial period. *Science,* 369 (6506), pp. 963-969. https://doi.org/10.1126/science.aay5538.

Hellstrom, J. 2006. U–Th dating of speleothems with high initial 230Th using stratigraphical constraint. *Quaternary Geochronology,* 1 (4), pp. 289-295. https://doi.org/10.1016/j.quageo.2007.01.004.

Hellstrom, J. C. 2003. Rapid and accurate U/Th dating using parallel ion-counting multi-collector ICP-MS. *Journal of Analytical Atomic Spectrometry,* 18 (11), pp. 1346-1351. https://doi.org/10.1039/B308781F.

Hendy, C.H. 1971. The isotopic geochemistry of speleothems—I. The calculation of the effects of different modes of formation on the isotopic composition of speleothems and their applicability as palaeoclimatic indicators. *Geochimica et Cosmochimica Acta,* 35 (8), pp. 801-824. https://doi.org/10.1016/0016-7037(71)90127-X.

Rodríguez-Arévalo, J., Diáz-Teijeiro, M.F. & Castaño, S. 2011. Modelling and mapping oxygen-18 isotope composition of precipitation in Spain for hydrologic and climatic applications. in: Isotopes in Hydrology, Marine Ecosystems and Climate Change Studies (IAEA). Proceedings of an International Symposium, Monaco, pp. 171–177.

Rossi, C., Bajo, P., Lozano, R.P. & Hellstrom, J. 2018. Younger Dryas to Early Holocene paleoclimate in Cantabria (N Spain): Constraints from speleothem Mg, annual fluorescence banding and stable isotope records. *Quaternary Science Reviews,* 192, pp. 71-85. https://doi.org/10.1016/j.quascirev.2018.05.025.

Thomas, E.R., Wolff, E.W., Mulvaney, R., Steffensen, J.P., Johnsen, S.J., Arrowsmith, C., White, J.W.C., Vaughn, B. & Popp, T. 2007. The 8.2 ka event from Greenland ice cores. *Quaternary Science Reviews,* 26 (1-2), pp. 70-81. https://doi.org/10.1016/j.quascirev.2006.07.017.